

PAPER • OPEN ACCESS

Fermi surface of the chiral topological semimetal PtGa

To cite this article: B V Schwarze *et al* 2022 *J. Phys.: Condens. Matter* **34** 425502

View the [article online](#) for updates and enhancements.

You may also like

- [Topological nature of the node-arc semimetal PtSn₃ probed by de Haas-van Alphen quantum oscillations](#)
Y J Wang, D D Liang, M Ge *et al.*
- [Fermi surfaces of the topological semimetal CaSn₂ probed through de Haas van Alphen oscillations](#)
K A M Hasan Siddiquee, Riffat Munir, Charuni Dissanayake *et al.*
- [Shubnikov-de Haas and de Haas-van Alphen oscillations in Czochralski grown CoSi single crystal](#)
Souvik Sasmal, Gourav Dwari, Bishal Baran Maity *et al.*




IOP | ebooks™

Bringing together innovative digital publishing with leading authors from the global scientific community.

Start exploring the collection—download the first chapter of every title for free.

Fermi surface of the chiral topological semimetal PtGa

B V Schwarze^{1,2}, M Uhlarz¹, J Hornung^{1,2} , S Chattopadhyay^{1,*} , K Manna^{3,4},
C Shekhar³, C Felser³ and J Wosnitzer^{1,2}

¹ Hochfeld-Magnetlabor Dresden (HLD-EMFL) and Würzburg-Dresden Cluster of Excellence ct.qmat, Helmholtz-Zentrum Dresden-Rossendorf, 01328 Dresden, Germany

² Institut für Festkörper- und Materialphysik, Technische Universität Dresden, 01062 Dresden, Germany

³ Max Planck Institute for Chemical Physics of Solids, 01187 Dresden, Germany

⁴ Indian Institute of Technology Delhi, Hauz Khas, New Delhi 110016, India

E-mail: s.chattopadhyay@hzdr.de

Received 3 March 2022, revised 10 June 2022

Accepted for publication 8 August 2022

Published 22 August 2022



CrossMark

Abstract

PtGa is a topological semimetal with giant spin-split Fermi arcs. Here, we report on angular-dependent de Haas–van Alphen (dHvA) measurements combined with band-structure calculations to elucidate the details of the bulk Fermi surface of PtGa. The strong spin–orbit coupling leads to eight bands crossing the Fermi energy that form a multitude of Fermi surfaces with closed extremal orbits and results in very rich dHvA spectra. The large number of experimentally observed dHvA frequencies make the assignment to the equally large number of calculated dHvA orbits challenging. Nevertheless, we find consistency between experiment and calculations verifying the topological character with maximal Chern number of the spin-split Fermi surface.

Supplementary material for this article is available [online](#)

Keywords: topological semimetal, Fermi surface, quantum oscillation

(Some figures may appear in colour only in the online journal)

1. Introduction

In recent years, the field of topology in condensed-matter physics has developed rapidly. Under certain circumstances, topological properties evolve from the electronic band structure of solids and lead to topologically protected states and quasiparticle excitations—opening a possible route to future quantum technology [1–3]. First to mention here are topological insulators with protected conducting edge and surface states [1]. Furthermore, the discovery of Weyl and

Dirac fermions in three-dimensional crystals spurred the field [3–19]. Besides these quasiparticles, that possess analogous fundamental particles in high-energy physics, new types of excitations are possible that are unique to solid-state materials [20–24]. Realizations of such excitations are multifold fermions that were evidenced using different experimental techniques very recently [25–31].

Multifold fermions are protected by chiral crystal symmetry and may have a topological charge with Chern number up to ± 4 . This large Chern number leads to associated long Fermi arcs that are much larger and more robust than those observed in Weyl semimetals with Chern number ± 1 . Materials that host multifold fermions with maximum Chern number are found in compounds with space group $P2_13$ (No. 198) [25–31].

We have recently reported on a comprehensive investigation of the chiral semimetal PtGa that demonstrates the

* Author to whom any correspondence should be addressed.



Original Content from this work may be used under the terms of the [Creative Commons Attribution 4.0 licence](#). Any further distribution of this work must maintain attribution to the author(s) and the title of the work, journal citation and DOI.

strongest spin-orbit coupling (SOC) observed so far in above class of materials [31]. Indeed, this material hosts a large number of Weyl points and nontrivial Weyl nodal walls with large net chiral charges [32]. We reported the first observation of the maximal Chern number 4, predominantly focusing on our angle-resolved photoemission-spectroscopy results together with preliminary magnetic quantum-oscillation data and band-structure calculations [31]. However, in that study, we measured de Haas–van Alphen (dHvA) data only for a few selected magnetic-field orientations along high-symmetry directions up to 7 T and down to 1.8 K. Thus, we had access only to those dHvA frequencies, which are below 700 T. Therefore, we could assign only a few expected dHvA orbits to the measured oscillations.

In this work, we report on a detailed angular-dependent quantum-oscillation study of PtGa up to 13 T and down to 0.5 K. By analyzing our experimental data thoroughly, we resolve extremely rich dHvA spectra in PtGa. Despite the inherent complexity of the spectra arising from the large number of experimentally observed frequencies, our calculated dHvA frequencies are consistent with the experimental ones and provide as well a rich set of Fermi-surface orbits. Our finding on the intricate details of the bulk Fermi surface of PtGa is an important extension of the existing knowledge on this chiral topological semimetal as it provides a broader understanding of the electronic structure of such kind of materials.

2. Methods

For the PtGa crystal-growth procedure from the melt, we used the self-flux technique as described in [31] in detail. We investigated the same PtGa single crystal as studied by magnetization experiments at lower fields previously [31]. We performed dHvA measurements over a broad angular range in a ^3He cryostat using a capacitive torque magnetometer up to magnetic fields of 13 T. The observation of clear quantum oscillations in our torque signals, appearing already at about 1.3 T at 0.5 K, reflects the very high quality of the investigated single crystal. Compared to the dHvA data we obtained previously by use of a SQUID (superconducting quantum interference device) magnetometer [31], the torque technique allows us to apply much higher magnetic fields and to measure down to lower temperatures. Further, the sensitivity of this technique grows with magnetic field, making torque magnetometry particularly advantageous for dHvA studies at high magnetic fields. Combined with the possibility to rotate the sample, we, therefore, were able to perform a more comprehensive dHvA study of PtGa. One should note, however, that a dHvA signal in torque measurements appears only for anisotropic Fermi surfaces, i.e. the signal is proportional to the derivative of the extremal area with respect to angle and becomes zero for a spherical Fermi surface.

We conducted density-functional-theory (DFT) calculations using the full-potential local orbit minimum basis code

(FPLO, version 15.02) [33] to calculate the band structure, Fermi surfaces, effective masses, and to account for the experimentally detected dHvA frequencies. Due to the strong SOC we applied a fully relativistic formalism [34] choosing the local density approximation of Perdew and Wang for the exchange-correlation potential [35]. We used a $40 \times 40 \times 40$ regular k -point mesh for the calculation of the band structure. For the calculation of the Fermi surfaces, we employed a finer grid with 160 points per dimension.

3. Results and discussion

The inset of figure 1 shows a typical as-measured torque signal at 1.5 K with clearly resolved dHvA oscillations. In fact, there is practically no change in the overall dHvA oscillation patterns with temperature (T) except the expected diminishing of the oscillation amplitude with increasing T . The negligible field-dependent background contribution reflects a highly isotropic background magnetization in PtGa. The fast Fourier transform (FFT) of the data between 4 and 13 T reveals a very rich dHvA frequency spectrum, displayed in the main panel. Here, we labeled some of the peaks that we were able to assign clearly to calculated orbits of extremal areas on the various Fermi surfaces (described later).

We measured the dHvA signal at various angles by rotating the crystal from field aligned along [001] to [110] and from [110] to $[\bar{1}11]$ in steps of about 10° at 1.5 K. For all investigated field orientations, the oscillating torque signals and the rich Fourier spectra remain similar to those shown in figure 1. The symbols shown in figure 2 reflect the extracted dHvA frequencies for all investigated angles. Thereby, we color-coded those data that we could assign to extremal orbits of the calculated Fermi surfaces (see figure 3). The orbits labeled on the right and left sides of figure 2 are the same as those indicated in figure 1. Filled black circles denote spectral peaks that could originate from different calculated orbits and open grey circles are of very low amplitude, such as the small peaks between 800 and 1200 T shown in figure 1. Although some of these latter peaks may arise from real extremal orbits, they may as well be caused by higher harmonics, magnetic breakdown, magnetic interaction, or torque interaction [36].

As mentioned, we conducted fully relativistic band-structure calculations using the FPLO code. Four, with SOC eight, bands cross the Fermi energy, sometimes even multiple times (see also supplementary figure 4 in [31]). This leads to a multitude of Fermi-surface sheets, as shown in figure 3. We labeled the eight bands with Greek letters and up (down) arrows according to the SOC-induced up (down) shift of the bands. For these sheets, we determined the angular-dependent extremal areas, calculated the dHvA frequencies, and plotted them in figure 2 as color-coded solid lines. The extremal orbits of the α bands are labeled by a_i^σ , for the β bands by b_i^σ , for the γ bands by c_i^σ , and for the δ bands by d_i^σ , with i running from 1 to the maximum orbit number and σ being an up or down arrow according to the band shift.

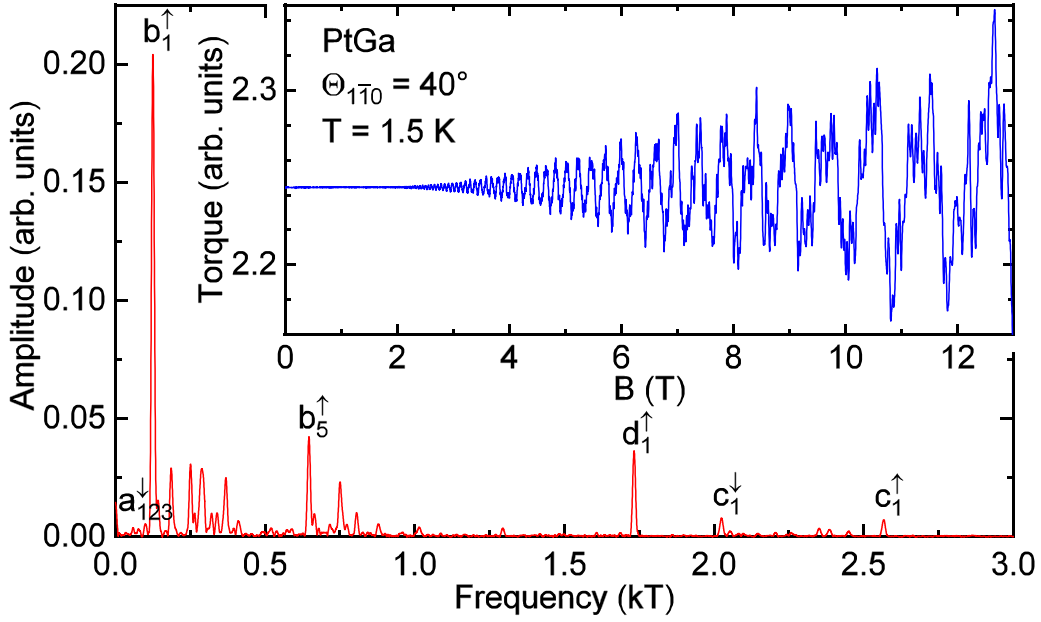


Figure 1. Fourier transform of the magnetic-torque data between 4 and 13 T shown in the inset, measured at 1.5 K and at $\Theta_{1\bar{1}0} = 40^\circ$, i.e. rotated by 40° from the [001] to the [110] axis.

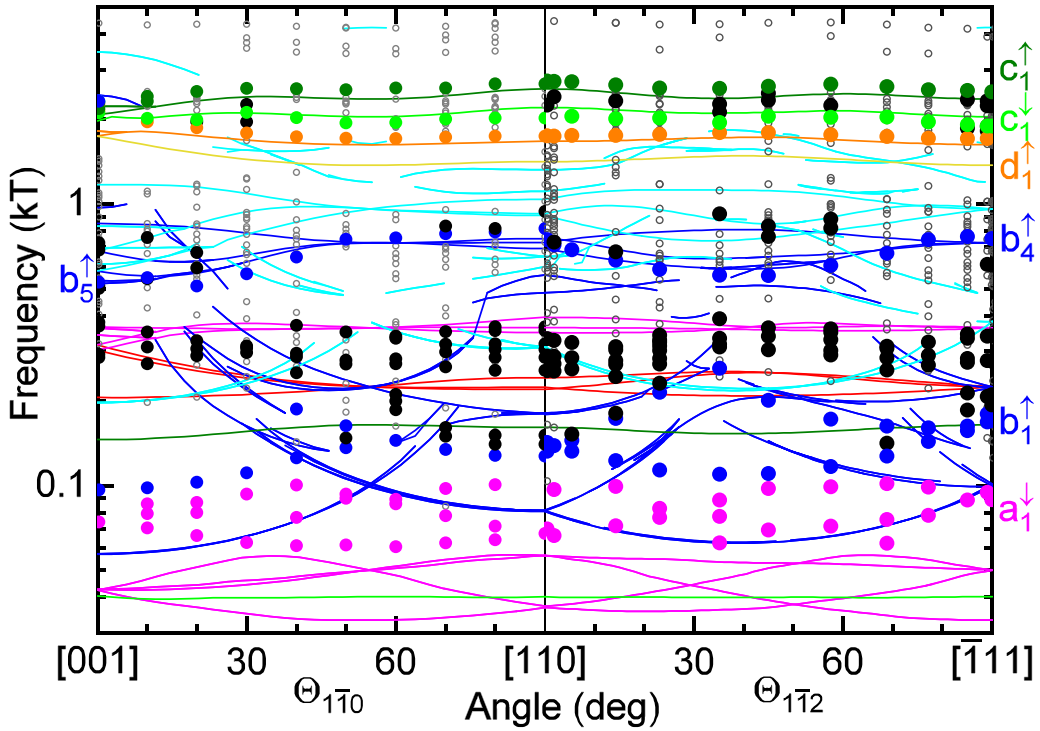


Figure 2. Angular dependence of experimentally observed (symbols) and calculated (lines) dHvA frequencies. The colors correspond to those of the calculated Fermi surfaces (see figure 3). Colored circles are assigned to the calculated orbits, solid black circles could not be unequivocally assigned, and small open grey circles represent FFT peaks with small amplitudes, i.e. with amplitudes less than about six times the noise level.

In line with the rich experimental dHvA spectra, we obtain a large number of calculated extremal orbits. This, however, makes a definite assignment of experimental dHvA frequencies to the calculated orbits challenging. For example, the observed dHvA frequencies between about 200 and 500 T

might originate from some orbits of the α or β bands. Accordingly, we used filled black circles for such not unequivocally assigned Fourier peaks in figure 2.

On the other side, there are a number of clearly resolved FFT peaks that fit well with predicted frequencies and their

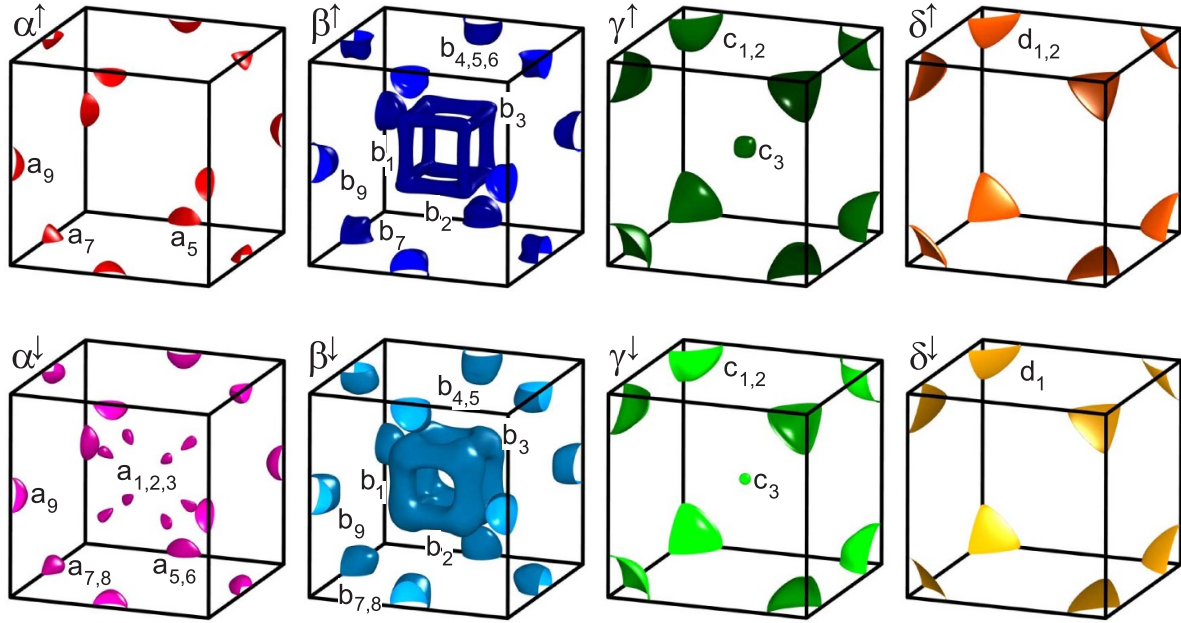


Figure 3. Calculated Fermi surfaces restricted to the first Brillouin zone. Each column shows the Fermi surfaces belonging to one of the four spin-split bands, α , β , γ , and δ , that cut the Fermi energy. The top row belongs to the spin-split bands shifted upward by SOC, the bottom row to the down-shifted spin-split bands. The up (down)-shifted bands are labeled by a superscript \uparrow (\downarrow). The calculated extremal orbits for field aligned along [001] are labeled by Roman letters and plotted next to the sheets where they occur (with up and down arrows omitted for better readability).

angular dependences. These peaks are shown as filled colored circles. The observed $a_{1,2,3}^\uparrow$ orbits, that originate from the small (magenta) ellipsoids near the center of the Brillouin zone (figure 3) and that lead to up to four angular-dependent dHvA orbits, are somewhat shifted to higher frequencies than calculated (from about 40–73 T). Although this might appear as a large discrepancy, especially in the semilogarithmic plot of figure 2, one should note that relative to the Brillouin-zone area perpendicular to the field, this is within the uncertainty of the DFT calculations. Similar applies for the (blue) b_1^\uparrow orbits. The experimental dHvA frequencies of the higher-frequency orbits, b_4^\uparrow , b_5^\uparrow , d_1^\uparrow , c_1^\uparrow , and c_1^\downarrow , fit very well to the calculated values.

In our torque data, the predicted dHvA frequency at about 40 T is not resolved. The corresponding c_3^\downarrow orbit (labeled α_1 in [31]) originates from the small (green) sphere around the Γ point of the γ^\downarrow band. This missing dHvA signal, most probably, is related to the almost ideal spherical shape of this orbit, with a calculated area change of less than 2.5% over the whole angular range. As mentioned, a dHvA signal in torque is only visible for an anisotropic Fermi surface. Consequently, the nearly ideal spherical shape of the c_3^\downarrow orbit leads to a vanishingly small torque oscillation. In the SQUID data [31], however, this orbit is well resolved.

Summarizing the comparison of measured and calculated dHvA frequencies, we can state that we find consistency between experiment and calculation. Tables 1 and 2 show a compilation of the measured and calculated dHvA frequencies for fields aligned along [001] and $[\bar{1}11]$, respectively.

As a next step, we determined the effective masses of all strong dHvA signals for these two field orientations ([001] and

$[\bar{1}11]$). As known from the Lifshitz–Kosevich (LK) formula [36, 37], the effective masses of the charge carriers are related to the temperature-dependent change of the dHvA oscillation amplitudes. The amplitude reduction for a fundamental dHvA oscillation is proportional to $X/\sinh X$, where $X = \alpha T m^*/B$, with the effective cyclotron mass m^* , given in multiples of the free electron mass m_e , and $\alpha = 2\pi^2 k_B m_e / (e\hbar) = 14.69 \text{ T K}^{-1}$. Thereby, k_B is the Boltzmann constant, e the electron charge, and \hbar the reduced Planck constant. When the oscillation amplitude is extracted by use of Fourier transformation, for B the harmonic mean of the magnetic-field window needs to be inserted. An overall error of about 5% could be assigned to our estimated effective masses.

Figure 4 shows, as an example, Fourier spectra of our torque data taken at some selected temperatures between 0.5 and 12 K for magnetic field parallel to $[\bar{1}11]$. The temperature-driven reduction of the Fourier peaks is obvious. The inset of figure 4 shows the temperature dependence of the labeled Fourier peaks, i.e. of the peaks that we could clearly assign to calculated orbits. The LK formula fits the data nicely (solid lines) and allowed us to extract the effective masses given in the legend. Here, we used data measured between $B_{\min} = 6 \text{ T}$ and $B_{\max} = 13 \text{ T}$, leading to a harmonic mean of $2/(B_{\min}^{-1} + B_{\max}^{-1}) = 8.21 \text{ T}$. We find relatively light effective masses, as expected for a semimetal without strong correlations. Most of the found values, between 0.21 and $0.82m_e$ are slightly larger than the calculated masses (table 2).

Previous studies showed that effective masses determined from Fourier analyses over extended field windows may be heavily underestimated [38, 39]. Indeed, the effective masses extracted from the Fourier spectra depend significantly on

Table 1. Experimentally determined dHvA frequencies and effective masses (m^*) as well as calculated frequencies and band masses (m_b) for magnetic field parallel to [001]. The effective masses m^* are determined for a field window between 6 and 13 T.

Orbit	Experimental		Calculated	
	F (T)	m^* (m_e)	F (T)	m_b (m_e)
c_3^\downarrow			40	0.08
$a_{1,2,3}^\downarrow$	74		43	0.13
b_1^\uparrow	97	0.17	57	0.16
c_3^\uparrow			146	0.20
b_1^\downarrow	193		197	0.24
a_9^\uparrow	264		206	0.15
$a_5^\uparrow, a_5^\downarrow$	284		303	0.19
$a_7^\uparrow, a_7^\downarrow$	293		315	0.20
a_6^\downarrow			343	0.21
a_8^\downarrow			363	0.23
a_9^\downarrow	372	0.24	366	0.23
b_5^\uparrow	511	0.27	522	0.25
b_6^\uparrow	528		534	0.28
$b_4^\uparrow, b_4^\downarrow$	543		578	0.26
b_2^\downarrow	618	0.29	612	0.47
$b_7^\uparrow, b_7^\downarrow$	687	0.35	681	0.31
b_5^\downarrow	710	0.37	699	0.34
b_8^\downarrow	795	0.48	835	0.41
b_9^\uparrow	898		852	0.42
b_2^\uparrow	978		970	0.79
b_9^\downarrow	1218		1173	0.56
$d_1^\uparrow, d_1^\downarrow$	2147	0.49	1745	0.51
d_2^\uparrow	2254	0.54	1815	0.51
c_2^\downarrow	2112	0.50	1971	0.59
$c_1^\uparrow, c_1^\downarrow$	2193	0.45	2073	0.55
c_2^\uparrow	2294	0.55	2228	0.61
b_3^\uparrow	2320	0.54	2438	1.24
b_3^\downarrow			3466	1.36

the chosen window size $w = 1/B_{min} - 1/B_{max}$. This is caused by the strong non-linear field dependence of the magnetic quantum oscillations, given mainly by the scattering rate on each orbit, i.e. by the Dingle temperatures [36]. Ideally, the window size w should be decreased to zero. This, however, reduces the dHvA frequency resolution by enlarging the Fourier-peak widths and leads to overlapping spectral peaks. We studied the window-size dependence of the extracted effective masses for some of the well-resolved FFT peaks to find an optimized and realistic window size based on the observed Fourier pattern in PtGa. We found that in PtGa, with a large number of rather dense Fourier peaks, the minimum w for a reliable analysis is limited to about 0.1–0.2 T⁻¹.

Figure 5 shows, how m^* , extracted by use of the LK formula, apparently increases when reducing the FFT window size. In order to estimate m^* for zero w , we used a smooth, heuristic formula, namely $m^* = m_0^* + m_1^* \exp(-w/b)$, with the three fit parameters m_0^* , m_1^* , and b . Obviously, the formula is

Table 2. Experimentally determined dHvA frequencies and effective masses (m^*) for a field range from 6 to 13 T as well as calculated frequencies and band masses (m_b) for magnetic field aligned along [111]. Effective masses labeled as m_{str}^* are extrapolated to zero Fourier-transformation window size.

Orbit	Experimental			Calculated	
	F (T)	m^* (m_e)	m_{str}^* (m_e)	F (T)	m_b (m_e)
a_1^\downarrow				33	0.12
c_3^\downarrow				40	0.08
$a_{2,3,4}^\downarrow$	92	0.21		50	0.15
b_1^\uparrow	163	0.30	0.42	100	0.29
c_3^\uparrow	189	0.33		164	0.23
b_2^\uparrow	210	0.36		223	0.56
$a_{5,7,9}^\uparrow$	276	0.17		224	0.55
$a_{5,7,9}^\downarrow$	340	0.22	0.27	363	0.21
b_1^\downarrow	382			382	0.61
$b_{4,7,9}^\uparrow$	754	0.43	0.49	728	0.37
$b_{4,7,9}^\downarrow$	884			960	0.48
d_1^\downarrow				1373	0.38
d_1^\uparrow	1885	0.39	0.58	1623	0.40
b_2^\downarrow	1623	0.82		1635	1.13
c_1^\downarrow	2323	0.58		2043	0.58
c_1^\uparrow	2501	0.66		2359	0.62
b_3^\downarrow	4210			4238	1.18

a very good description of the experimental data. Extrapolation to zero w gives us effective-mass values that, most probably, are closer to reality. Our analysis shows that even for our smallest window size (6–13 T), we may underestimate m^* by up to 38%.

Still, even these larger, extrapolated masses are well below $1m_e$ and only somewhat larger than the calculated ones (table 2). When comparing the experimental with the calculated effective masses (tables 1 and 2), some of the experimental values appear to be smaller than expected. This, most probably, is caused by the relatively large FFT window size necessary to obtain well-resolved Fourier peaks.

Concluding this part, we may state that the effective cyclotron masses in PtGa are only slightly enhanced with respect to the bare band masses m_b . This means that correlation effects play only a very minor role. The mass enhancement presumably may be well explained by some modest electron-phonon coupling.

We finally want to remark on the phase factor of the dHvA oscillations. In principle, the oscillating signal acquires an additional Berry phase, φ_B , when the electron orbit encloses a Weyl or Dirac point [40]. This Berry phase comes on top of other phase-factor contributions that are discussed theoretically in [41, 42] and for real data of the Weyl semimetal NbP in [43]. In the present case, we refrained from trying to determine the absolute phases, since, for a valid extraction, the dHvA signal of one individual frequency must be separated. In view of the extraordinarily rich frequency mix of the dHvA signal such an extraction cannot be done reliably for PtGa.

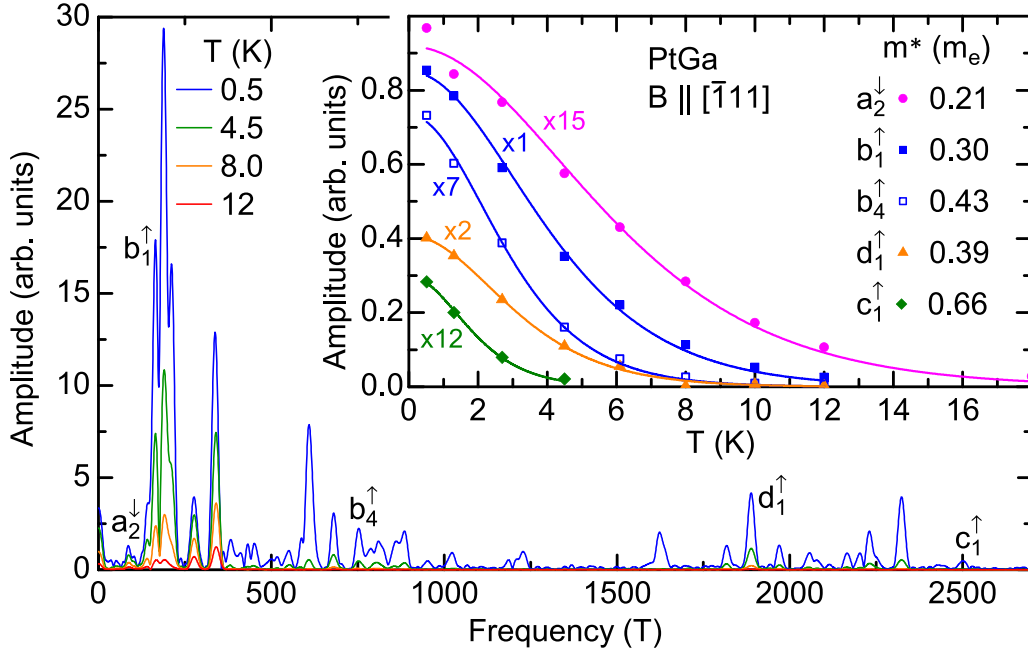


Figure 4. Fourier spectra of magnetic-torque data measured between 6 and 13 T with the magnetic field parallel to $[\bar{1}11]$ for selected temperatures. The inset shows the fits using the Lifshitz–Kosevich formula (solid lines) to the temperature-dependent amplitudes of the dHvA frequencies labeled in the main panel. The resultant effective masses, m^* , are given in the legend.

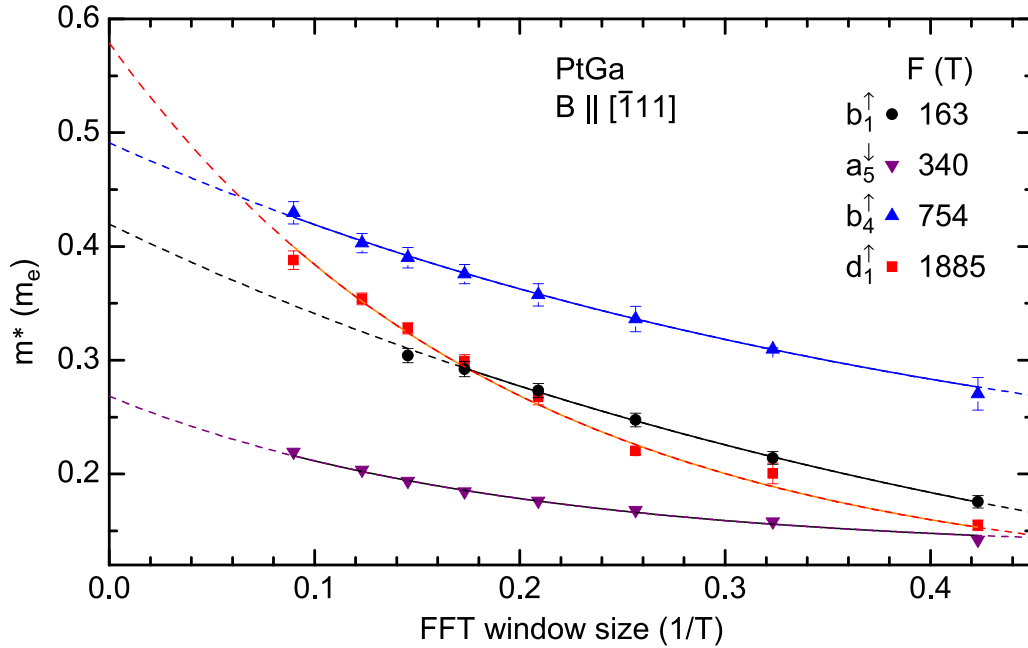


Figure 5. Dependence of the extracted effective masses on the window size used for the FFT. The maximum field value used is 13 T for all windows, the minimum ranges from 2 to 6 T. The lines are fits using the heuristic formula $m^* = m_0^* + m_1^* \exp(-w/b)$, with window size w and fit parameters m_0^* , m_1^* , and b . The dashed lines are extrapolations of the fits to zero.

4. Summary

In summary, we performed a comprehensive dHvA study combined with DFT calculations in order to determine the Fermi surface of the topological semimetal PtGa. We find a rather evolved Fermi-surface topology with a large number of extremal orbits caused by strong SOC that leads to eight

bands—instead of four without SOC—crossing the Fermi energy. By carefully analyzing the very rich dHvA spectra, we could reasonably well assign most of the various frequencies to calculated orbits. The experimentally determined effective cyclotron masses are slightly enhanced compared to the calculated band masses. In the process, we found a sizeable dependence of the effective masses on the chosen FFT window size.

Reducing this window size leads to apparent larger masses that are presumably closer to the real values. Altogether, we find that our experimental data are consistent with the DFT calculations. This further confirms the realization of a topological Fermi surface with maximal Chern number in PtGa.

Data availability statement

The data that support the findings of this study are available upon reasonable request from the authors.

Acknowledgments

The work was supported by the Deutsche Forschungsgemeinschaft (DFG) through the Würzburg-Dresden Cluster of Excellence on Complexity and Topology in Quantum Matter–*ct.qmat* (EXC 2147, Project No. 390858490) and SFB 1143, by the ANR-DFG under Grant Fermi-NES_t, and by Hochfeld-Magnetlabor Dresden (HLD) at HZDR, member of the European Magnetic Field Laboratory (EMFL). K M, C S, and C F acknowledge financial support from the European Research Council (ERC), Advanced Grant No. 742068 ‘TOP-MAT’; European Union’s Horizon 2020 research and innovation program (Grant Nos. 824123 and 766566). Additionally, K M acknowledges funding support from Max Planck Society under Max Planck-India partner group project and the Board of Research in Nuclear Sciences (58/20/03/2021-BRNS, DAE-YSRA), Department of Atomic Energy (DAE), Government of India.

ORCID iDs

J Hornung  <https://orcid.org/0000-0003-2718-7664>
S Chattopadhyay  <https://orcid.org/0000-0001-9061-2139>

References

- [1] Hasan M Z and Kane C L 2010 *Rev. Mod. Phys.* **82** 3045–67
- [2] Bansil A, Lin H and Das T 2016 *Rev. Mod. Phys.* **88** 021004
- [3] Armitage N P, Mele E J and Vishwanath A 2018 *Rev. Mod. Phys.* **90** 015001
- [4] Young S M, Zaheer S, Teo J C Y, Kane C L, Mele E J and Rappe A M 2012 *Phys. Rev. Lett.* **108** 140405
- [5] Liu Z K, Jiang J, Zhou B, Wang Z J, Zhang Y, Weng H M, Prabhakaran D, Mo S-K, Peng H, Dudin P 2014 *Nat. Mater.* **13** 677–81
- [6] Borisenko S, Gibson Q, Evtushinsky D, Zabolotnyy V, Büchner B and Cava R J 2014 *Phys. Rev. Lett.* **113** 027603
- [7] Neupane M et al 2014 *Nat. Commun.* **5** 3786
- [8] Liu Z K et al 2014 *Science* **343** 864–7
- [9] Weng H, Fang C, Fang Z, Bernevig B A and Dai X 2005 *Phys. Rev. X* **5** 011029
- [10] Xu S-Y et al 2015 *Science* **349** 613–7
- [11] Shekhar C et al 2015 *Nat. Phys.* **11** 645–9
- [12] Lv B Q et al 2015 *Phys. Rev. X* **5** 031013
- [13] Lv B Q et al 2015 *Nat. Phys.* **11** 724–7
- [14] Xu S-Y et al 2015 *Nat. Phys.* **11** 748–54
- [15] Xu N et al 2016 *Nat. Commun.* **7** 11006
- [16] Zhang C, Guo C, Lu H, Zhang X, Yuan Z, Lin Z, Wang J and Jia S 2015 *Phys. Rev. B* **92** 041203(R)
- [17] Liu Z et al 2016 *Nat. Mater.* **15** 27–31
- [18] Hasan M Z, Xu S-Y, Belopolski I and Huang S-M 2017 *Annu. Rev. Condens. Matter Phys.* **8** 289–309
- [19] Yan B and Felser C 2017 *Annu. Rev. Condens. Matter Phys.* **8** 337–54
- [20] Bradlyn B, Cano J, Wang Z, Vergniory M G, Felser C, Cava R J and Bernevig B A 2016 *Science* **353** 1–7
- [21] Mañes J L 2012 *Phys. Rev. B* **85** 155118
- [22] Chang G et al 2017 *Phys. Rev. Lett.* **119** 206401
- [23] Tang P, Zhou Q and Zhang S-C 2017 *Phys. Rev. Lett.* **119** 206402
- [24] Zhang T, Song Z, Alexandradinata A, Weng H, Fang C, Lu L and Fang Z 2018 *Phys. Rev. Lett.* **120** 016401
- [25] Takane D et al 2019 *Phys. Rev. Lett.* **122** 076402
- [26] Sanchez D S et al 2019 *Nature* **567** 500–5
- [27] Rao Z et al 2019 *Nature* **567** 496–9
- [28] Schröter N B M et al 2019 *Nat. Phys.* **15** 759–65
- [29] Schröter N B M et al 2020 *Science* **369** 179–83
- [30] Rees D, Manna K, Lu B, Morimoto T, Borrmann H, Felser C, Moore J E, Torchinsky D H and Orenstein J 2020 *Sci. Adv.* **6** eaba0509
- [31] Yao M et al 2020 *Nat. Commun.* **11** 2033
- [32] Ma J-Z et al 2021 *Nat. Commun.* **12** 3994
- [33] Koepnick K and Eschrig H 1999 *Phys. Rev. B* **59** 1743–57
- [34] Eschrig H, Richter M and Opahle I 2004 *Relativistic Electronic Structure Theory: Part 2. Applications (Theoretical and Computational Chemistry vol 14)* ed P Schwerdtfeger (Amsterdam: Elsevier) pp 723–76
- [35] Perdew J P and Wang Y 1992 *Phys. Rev. B* **45** 13244–49
- [36] Shoenberg D 1984 *Magnetic Oscillations in Metals* (London: Cambridge University Press)
- [37] Lifshitz I M and Kosevich A M 1956 *Sov. Phys. -Usp.* **2** 636–45
- [38] Audouard A and Fortin J 2018 *Eur. Phys. J. Appl. Phys.* **83** 30201
- [39] Schindler C, Noky J, Schmidt M, Felser C, Wosnitza J and Gooth J 2020 *Phys. Rev. B* **102** 035132
- [40] Mikitik G P and Sharlai Y V 1999 *Phys. Rev. Lett.* **82** 2147–50
- [41] Alexandradinata A, Wang C, Duan W and Glazman L 2018 *Phys. Rev. X* **8** 011027
- [42] Alexandradinata A and Glazman L 2018 *Phys. Rev. B* **97** 144422
- [43] Schindler C, Gorbunov D, Zherlitsyn S, Galeski S, Schmidt M, Wosnitza J and Gooth J 2020 *Phys. Rev. B* **102** 165156